PROCEEDINGS, 48th Workshop on Geothermal Reservoir Engineering
Stanford University, Stanford, California, February 6-8, 2023
SGP-TR-224

Nanoparticle-based tracing techniques in geothermal reservoirs: Advances, challenges and prospects

Laura Spitzmüller[1], Fabian Nitschke[1], Annika Maercks[1], Jonathan Berson[2,3], Bastian Rudolph[1], Thomas Schimmel[2,3], Thomas Kohl[1]

[1] Dept. Geothermal Energy & Reservoir Technology, Karlsruhe Institute of Technology (KIT), Adenauerring 20b, 76131 Karlsruhe, Germany. [2] Institute of Nanoscience, Karlsruhe Institute of Technology (KIT), Hermann-von-Helmholtz-Platz 1, 76344 Eggenstein-Leopoldshafen, Germany. [3] Institute of Applied Physics, Karlsruhe Institute of Technology (KIT), Wolfgang-Gaede-Straße 1, 76131 Karlsruhe, Germany.

laura.spitzmueller@kit.edu

Keywords: functional nanoparticles, nanotracer, stability, dissolution, surface modification, sorption control

ABSTRACT

Accurate knowledge of reservoir geometry and flow paths are critical parameters for successful geothermal operations. They are essential for evaluating the long-term behavior and sustainability of geothermal reservoirs. Conventional hydraulic testing and tracer tests are often inconclusive or provide limited information due to complex and challenging reservoir conditions (multiple well systems, complex reservoir geometry, and fracture network, etc.). Recently, a new class of tracer techniques has emerged in order to overcome the major drawbacks of molecular tracers: nanoparticle-based tracers. The main advantages of nanoparticle tracers compared to molecular tracers are their tunable properties and modular structure. Functional and smart nanoparticle tracers such as the threshold-triggered temperature nanotracer enabled the simultaneous evaluation of multiple reservoir conditions (flow paths, temperature distribution, etc.) and created an entirely new field of research. As new areas of research often require detailed insights into fundamental processes, there are still open questions about the interactions between particles, fluids, and rock minerals and their performance in complex geothermal environments. As an example, the application of embedded or surface-bound tracing features (e.g., fluorescent molecules, DNA, etc.) within or on a silica matrix prevents the tracing function from being affected by the environment (e.g., pH changes, salinity effects, redox sensitivity). Although silica has low hydro(thermal) stability and loses its protective function at high temperatures or long-term applications, nanoscience offers a comprehensive set of tools to design and protect the silica matrix. Another advantage is the possibility of surface modifications, which can help to achieve minimum sorption and retention by adapting the ζ-potential of the nanoparticles. In this study, we address recent advances in increasing long-term stability, improving hydrothermal stability of silica nanoparticles, sorption control. Furthermore, we present strategies for the development and functionalization of nanoparticle-based tracers.

1. INTRODUCTION

Successful development and operation of geothermal power plants require detailed characterization of subsurface reservoir properties, such as its geometry and flow paths. Their exploration is conducted so far with well-established tracer techniques that usually rely on molecular dyes such as uranine or eosin. However, molecular dyes can be greatly affected by the fluids pH, temperature and the rock properties of the underground (Maier et al., 2015). This can lead to thermal degradation and mineral surface adsorption and in extreme cases to complete retention of molecular tracers and impedes effective multi-well tests using multiple tracers as each molecule possesses different sorption characteristics. Thus, there is the requirement for new approaches to overcome the drawbacks of the molecular dyes and utilize the additional functionalities a particle-based approach would provide. Unlike molecules, however, nanoparticles facilitate the design of a much more complex and reactive system. Particularly silica nanoparticles have proved to combine many favorable properties. They are comparatively easy to synthesize in a wide range of sizes. They can be built up modularly, while the particles properties and functionalities are tunable. The control of porosity enables the control of surface area. Basic research has been conducted on the application of silica nanoparticles as tracers in hydrology for aquifer and reservoir assessment (Vitorge et al., 2014). Further developments led to advanced temperature-sensitive silica nanoparticles as tracers in controlled environments for geothermal reservoir characterization (Puddu et al., 2016; Rudolph et al., 2020) Indeed, nanoparticle-based approaches to geothermal applications have so far been limited in the scope of their application. For example, DNA-embedded silica nanoparticle tracers could only be successfully employed at test sites with low temperature groundwater and distances of only a few meters between the injection and the extraction points (Kong et al., 2018; Mikutis et al., 2018, Kittilä et al., 2019). While some studies aim at temperature detection functionality (Puddu et al., 2016), other experiments at elevated temperatures contradict the viability of the application, where a simple experimental setup with Milli-Q water, quartz sand and temperatures of 150 °C resulted in high sorption rates and degradation of the nanoparticles (Zhang et al., 2016). The shortcomings in laboratory studies and application failures of the technology are always attributed to the lack of understanding of the fundamental geochemical interaction processes at the interfaces of the particle to the fluid and the reservoir rock mineral.

Within this study, we first present a new type of silica nanoparticle tracer that enables simultaneous flow path and temperature detection. The proof of concept is given by laboratory-scale flow through experiments where the nanoparticle tracer proofed to be as effective as uranine and shows better transportation properties than eosin. We also address the problem of silica (in)stability in aqueous environments and examine the impact on our particle system and evaluate sorption processes. We further provide stabilization and sorption control methods and proof their applicability and effectivity.

2. NANOPARTICLE TRACERS

The nanoparticle tracers are built in a 3-layer architecture to enable simultaneous flow path detection and temperature sensing. The fluorescent core (Fig. 1a) is designed to remain stable throughout the tracer test procedure and serves as a reference function to detect tracer retrieval. The second layer, a mesoporous shell doped with a second fluorophore, serves as the (temperature) reporting unit (Fig. 1c), while the third layer, the shell, is responsible for the temperature-triggered activation of the nanotracers (Fig. 1d). The nanotracer structuring process described here is modular, i.e., the sizes, materials, dyes, and temperature-dependent shell can be changed.

2.1 Synthesis

To synthesize the core, a reversed micro-emulsion synthesis with simultaneous incorporation of a fluorescent dye is performed (Fig 1a). First, 15 mL cyclohexane (VWR Chemicals AnalaR Normapur), 3.44 mL n-hexanol (VWR GPR Rectapur, 98 %) and 3.44 mL Triton X-100 (Sigma Aldrich, analysis grade) are mixed and stirred until the solution is clear. Then, 0.96 mL of a 20 mM aqueous Tris(2,2-bipyridyl)dichlororuthenium(II) hexahydrate ($Ru(bpy)_3^{2+}$, Acros organics, 98%) solution and 0.2 mL tetraethyl orthosilicate (TEOS, Sigma Aldrich, 99 %) are added to the mixture. After 20 minutes of stirring, 0.12 mL ammonium hydroxide solution (Merck, 28-30 %) is added. The solution is further stirred for 24 hours before adding 28 mL acetone (VWR Chemicals, 99.8 %) to break the micro-emulsion. The nanoparticles are collected by centrifugation (5 minutes at 16k*g) and subsequently washed with acetone, twice with ethanol (VWR Chemical, 99.9 %) and deionized water. In a second step, the mesoporous shell is formed in a sol-gel process with silica-precursor TEOS and CTAB-micelles as template (Fig 1b, grey shell with dark grey radial pores). First, an aqueous 0.2 M cetyltrimethylammonium bromide (CTAB, Merck, 97 %) solution is prepared and kept for 24 hours under constant stirring. The core-nanoparticles (Fig. 1a) are dispersed using a sonotrode (Hielscher Ultrasond) in 6 mL Millipore water and added to 60 mL of the CTAB-solution under constant stirring for 30 minutes. The particles are then collected by centrifugation and re-dispersed in 60 mL Millipore water using a sonication bath and a vortex. 0.6 mL of an aqueous 0.1 M sodium hydroxide (NaOH, Sigma Aldrich) solution is added to the mixture. To grow the silica shell (light grey shell in Fig 1b), 3 times 180 µL of 20 % v/v TEOS in methanol (VWR Chemicals, 99.9 %) are added dropwise over 30 minutes, i.e. 180 µL every 10 minutes). After 48 hours stirring the nanoparticles are re-collected by centrifugation (10 minutes 16k*g), followed by three washing-centrifugation cycles, two using water and the last with methanol. The particles now have a fluorescent core and a mesoporous shell, which is depicted in Fig 1b. To remove the CTAB micelles from the pores and subsequently fill them with a second fluorophore (Fig 1c), the particles are in a next step re-suspended in methanol. The extraction of the CTAB micelles is performed under reflux at 70 °C. At first, the particles are added to a mixture of 120 mL methanol, 2.48 mL H_2O and 1.24 mL hydrochloric acid (HCl, Fluka, 36.5-38 %) and heated to 70 °C under constant stirring. The mixture is refluxed for 24 hours. The particles are then re-collected by centrifugation and washed two times with methanol and one time with ethanol. In a next step, the particles are dried under vacuum and weighed. 2.9 mg Safranin O (Acros organics, 95 %) is added per 10 mg of nanoparticles. The particles and the dye are then stored under nitrogen atmosphere for at least 2 hours. Then, 0.5 mL dry acetonitrile (Merck, 99.5 %) is added per 10 mg of nanoparticles. The solution is stirred under nitrogen atmosphere for 16 hours. The stirring of dye and particles in dry acetonitrile enables the adsorption of the dye molecules inside the pores of the nanoparticles (Fig 1c). Finally, the solution is taken out from the nitrogen atmosphere and exhibited to the ambient atmosphere. 75 µL n-Octadecyltrimethoxysilane (abcr GmbH, 95 %) is added per 10 mg of nanoparticles to enable the adsorption of the protective hull. The solution is stirred for 16 hours, the particles are then collected by centrifugation and washed with acetonitrile and hexane (VWR Chemicals, 99 %), followed by vacuum drying. The dried particles are re-suspended in 40 mL hexane and 75 mg of the desired paraffin is added as temperature-responsive hull. E.g., tetracosane (Sigma Aldrich, 99 %, T_t 50 °C), dotriacontane (Sigma Aldrich, 97 %, T_t 70 °C) and tetratetracontane (Sigma Aldrich, 99 %, T_t 90 °C) were used successfully as capping agents. The mixture of nanoparticles in hexane with added paraffin is sonicated for 15 minutes and stirred for 15 minutes, followed by collecting the particles via centrifugation and dried in vacuum. The paraffin-coated nanoparticles (Fig 1d) are re-suspended in water with 10 mg mL^{-1} sodium dodecyl sulfate (SDS) and washed until the supernatant is clear. The temperature-responsive nanotracers are then ready for usage. SEM images of the different synthesis steps are depicted in Fig 1e and Fig 1f and show the initial core with a size of about 50 nm and the final nanoparticle tracer with a size of about 70 nm.

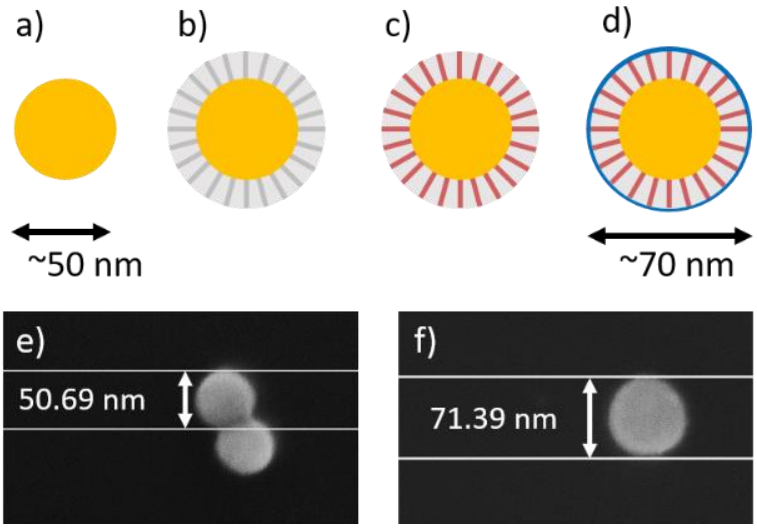

Figure 1. Schematic structure of the nanoparticle tracer synthesis (a-d) and respective SEM-images (e-f) of state a) and d). At first, the core incorporating a fluorophore is synthesized (a). Then, a mesoporous shell is grown on the core using CTAB micelles as template (b). Further, the micelles are removed and the pores are filled with a second fluorophore (c). To enable a temperature-triggered release of the second dye, the pores are sealed with a temperature-sensitive pore blocker (d). e) and f) show the size comparison of the core (e) and the functionalized nanotracer (f).

2.2 Function principle

The working principle of the temperature-triggered nanoparticle tracers is shown in Fig. 2a-c. The nanotracers were coated with paraffin during synthesis, which enables their threshold-triggered activation. Paraffins have a certain threshold temperatures (T_t) above which the paraffin begins to melt and, in our case, releases the pristine surfaces to the surrounding medium. Due to the irreversible loss of the protective function of the shell, the dye safranin O is released from the mesoporous shell (Fig. 2b). Finally, the reacted particles contain only the $Ru(bpy)_3^{2+}$ dye, while the unreacted particles contain both the $Ru(bpy)_3^{2+}$ and safranin O dyes. The difference between the unheated, i.e., unreacted, and the heated, i.e., reacted, particles can be observed optically (Fig. 2d) based on the color change and/or analytically with a fluorescence spectroscope (Fig. 2e). Since $Ru(bpy)_3^{2+}$ and safranin O both emit at the same wavelength (612 nm), they can be measured simultaneously, which facilitates the analysis of the state of the particles (reacted/unreacted).

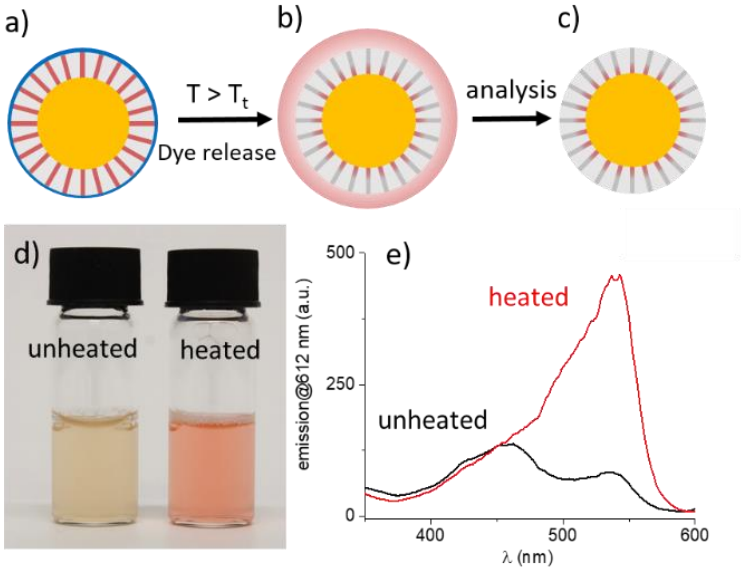

Figure 2: Function principle of the temperature-triggered nanoparticle tracers. A) to c) show the reaction of the nanoparticle tracers to elevated temperatures. At first, the particles are coated with a temperature triggered hull (a) which prevents the dye in the shell to leak. When the temperature threshold (T_t) of the hull is exceeded, the hull breaks and subsequently the dye in the shell is released (b). Thus, the reacted nanotracers (c) finally only contain the dye incorporated in the core. The difference between

unheated, i.e. not reacted and heated, i.e. reacted nanoparticle tracers can be distinguished optically (d) and/or can be identified using fluorescence spectroscopy (e).

2.3 Proof of concept

To demonstrate the applicability of the nanoparticle tracers, flow tests were carried out at ambient temperature with a 1 m long packed column (inner diameter 53 mm) with coarse quartz sand (1.0 - 1.6 mm diameter). The column is coated with epoxy and quartz sand to prevent the formation of channels along the wall surfaces. The outlets are sealed with sintered glass (mesh size 160 – 250 µm). To allow a continuous flow-through analysis cycle, the outlet of the column is connected via a tube to a flow-through quartz cuvette in a fluorescence spectrometer. A constant flow of 4 mL s^{-1} is maintained by placing a column filled with water 0.87 m (hydraulic gradient) above the inlet of the sand-filled column, which is automatically refilled. The effective porosity of the sand-filled column can be estimated at 28 % (Stephens et al., 1998). The hydraulic conductivity (K) can be calculated using Darcy's law and is $2.08*10^{-3}$ m/s, flow velocity (u) is $6.5*10^{-3}$ m/s, permeability (k) is $2.13*10^{-10}$ m^2, and the diffusion coefficient is $6.12*10^{-12}$ m^2/s.

The tracers are injected with a syringe through a septum 16 cm upstream from the inlet of the sand-packed column. The performance of the nanoparticle tracers is compared with conventional molecular tracers, namely uranine and eosin. The breakthrough curves are shown in Figure 3a. All three tracers tested are retrieved and detected by fluorescence spectroscopy. However, they show significantly different behavior. While the nanoparticle tracer and uranine have almost the same T_{min}, eosin is significantly retarded. In addition, the T_{peak} of eosin is later than the T_{peak} of uranine and the nanoparticles, and the tailing of eosin is more pronounced (no baseline was reached within 60 minutes). Uranine and the nanoparticles behave almost ideally, with sharp peaks and low tailing. A magnification of the breakthrough curves between 2 and 8 minutes after injection of the tracers is shown in Figure 3b. It can be noted that although T_{min} of uranine is slightly smaller than T_{min} of the nanoparticles, the nanoparticles have a sharper breakthrough curve and lesser tailing. This could be an indication of the lower diffusion of the nanoparticles, which experience size exclusion effects and tend to stay in the main streamlines. The retrieval rates are calculated using intensity-to-concentration calibration curves, flow velocity, and the input concentration. The retrieval of the nanoparticles is about ten times higher than the retrieval of eosin (Table 1), however still not reaches the retrieval rate of uranine. These results indicate possible sorption phenomena or retention of the nanotracers and raises the question of the effect of particle-mineral surface interactions.

Table 1: Results of the flow through experiments with different tracers T_{min}, T_{max}, v_{max} and v_{peak} are directly derived from the breakthrough curves, the retrieval rate is calculated using the input concentration, the cumulated output concentration and the flow rate.

Tracer	T_{min} (s)	T_{peak} (s)	V_{max} (10^{-3} m/s)	V_{peak} (10^{-3} m/s)	Retrieval rate (%)
Nanoparticles	171	264.6	5.8	3.8	78.5
Uranine	155.4	250.5	6.4	4.0	96.8
Eosin	250.2	494.4	4.0	2.0	8.2

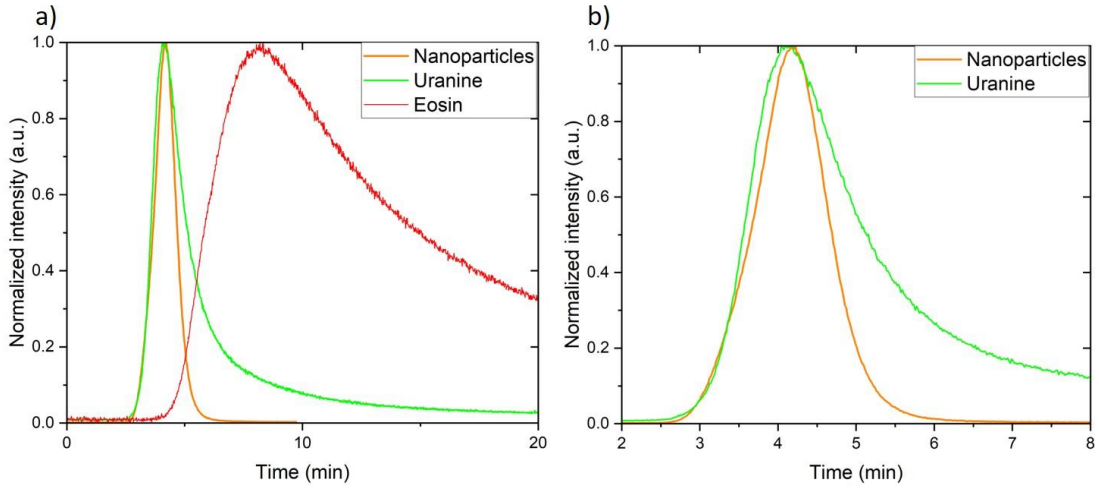

Figure 3: Breakthrough curves of tracers through a 1m packed column with coarse quartz sand. A) shows the normalized breakthrough curves of the nanoparticle tracers, uranine and eosin. In b) a magnification of the breakthrough curves of nanoparticles and uranine is shown.

3. APPLICATION RELATED CHALLENGES AND ADVANCES

3.1 Hydrothermal (in)stability

A few challenges must be overcome before the nanoparticle tracers can be applied successfully. The main challenge is the hydrothermal (in)stability of the silica nanoparticles themselves. Both the core and the shell are composed of silica and therefore dissolve in aqueous solutions due to the nucleophilic attack of the surface silanol groups (Si-OH) (Cypryk and Apeloig, 2002). The dissolution is particularly problematic for the core, as the core must stay stable to be detected after passing through a reservoir to provide the information about successful retrieval of the particles. The dissolution behavior of amorphous silica in water has been extensively studied (e.g., Alexander et al., 1954, Iler, 1979, Crundwell, 2017); however, the behavior of artificial silica nanoparticles is not yet fully understood. There is contradicting literature on the (in)stability of such nanoparticles in aqueous media (including biomedical/pharmaceutical applications), which may also be due to experimental conditions (e.g., Alaskar et al., 2015, Mikutis et al., 2018, Jafari et al., 2019, Möller and Bein, 2019). For example, particle concentration, temperature, pH, degree of condensation of the network, surface modification, and choice of analytical methods (e.g., aquatic analysis vs. dynamic light scattering) all play an important role in correctly determining the dissolution rate and can lead to incorrect conclusions. Figure 4a shows the result of a dissolution experiment with 1 mg mL^{-1} silica nanoparticles without surface modifications at room temperature and without fixing pH. The dissolution is monitored by UV-VIS measurement of the solution using the molybdenum blue method. This method explicitly analyzes only the dissolved silica (monomers, subordinated dimers) in solution and does not react with the particles or the surface of the particles (Iler, 1979). Dissolution of the silica nanoparticles begins immediately after contact with the aqueous solution and progresses until equilibrium is reached (Fig. 4a). This equilibrium is the saturation concentration of the silica and depends on several factors, such as the temperature, pH, and salinity of the solution. The effect of dissolution can be carefully analyzed using SEM/TEM devices. Figure 4b and c show SEM images of pristine, undisturbed silica nanoparticles (Fig. 4b) to partly dissolved silica nanoparticles (Fig. 4c). A comprehensive study on the dissolution behavior of silica nanoparticles in different aqueous media with special attention to the impact of different factors (e.g. particle concentration, availability of silica, pH, etc.) can be found in Spitzmüller et al. (2023).

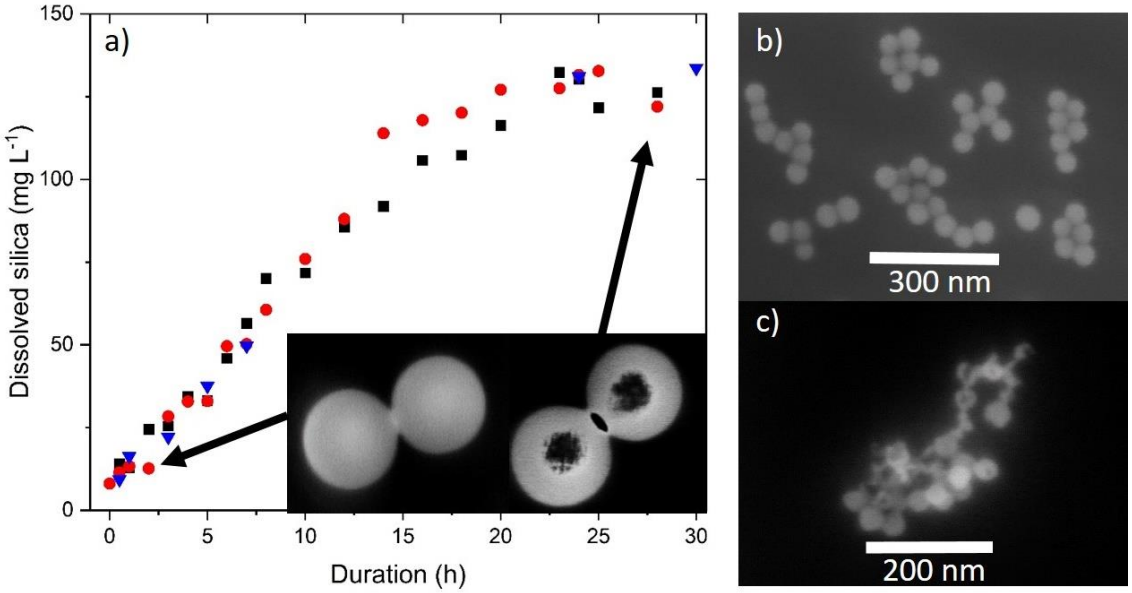

Figure 4: Dissolution of the silica nanoparticles in water over time at room temperature. A) On the y-axis the concentration of dissolved silica is shown. The saturation of (amorphous) silica at ambient conditions is in the range of 90 mg/L to 150 mg/L (Iler, 1979). Inset of SEM images showing the undisturbed nanoparticles (SEM image left) and dissolution/disintegration of the particles (SEM image right) before and after 28 hours exposure to aqueous solution. B) SEM image of the undisturbed nanoparticles. C) SEM image of partly dissolved and disintegrated nanoparticles after 1 day in aqueous solution.

3.2 Stability improvement strategies

To prevent the nanotracers from dissolution and degradation, we tested several surface modifications to improve the stability of the silica network. An overview of the most effective strategies is displayed in Figure 5a by monitoring the dissolution of silica over a 4-week exposure of 1 mg mL^{-1} nanoparticles to aqueous media. As expected, the untreated particles (Fig. 5a black square) suffer immediate dissolution and equilibrate as soon as the silica saturation concentration in solution is reached. Chemical surface modification strategies such as silanization (octadecyltrimethoxysilane, Fig 5a light blue hexagon) and paraffin coating (dotriacontane, Fig 5a olive square) proofed to lower the nanoparticle dissolution and seem to equilibrate at silica concentrations below 50 mg L^{-1} within 4 weeks at room temperature. Another approach on stabilizing is the coating with a metal oxide, in our case, titania (Fig. 5a pink triangle). The titania hull has a similarly stabilizing effect on the nanoparticles as silanization and paraffin coating. However, the by far most effective method stabilizing silica nanoparticles turned out to be calcination (Fig. 5a, red dot, blue triangle). Due to condensation processes at high temperatures, the silica network is stronger linked and can resist the nucleophilic attack of the water. The success of the surface

modifications is proofed via FT-IR ATR spectroscopy (Fourier-Transform Infrared Spectroscopy Attenuated Total Reflectance, Fig. 5b). FT-IR ATR spectroscopy is commonly used to identify chemical bonds based on their unique bending and stretching vibrational characteristics in the infrared wavelength region. Important wavenumbers for silica nanoparticles are 1100 – 1000 cm^{-1} for asymmetric Si-O-Si (siloxane) stretching, 802 cm^{-1} for symmetric siloxane wagging, 455 cm^{-1} for siloxane bending vibration, and 970 cm^{-1} for Si-OH (silanol) stretching (Socrates, 2004, Widjonarko et al., 2014). Other important information can be identified in the region of 3700 – 3200 cm^{-1}, vibrations can be assigned to stretching of adsorbed OH molecules (Widjonarko et al., 2014). Silanized samples further exhibit CH_3 stretching in the region of 3000 – 2800 cm^{-1}, asymmetric C-H bending at 1450 cm^{-1} and symmetric C-H bending at 1400 cm^{-1} (Zeitler and Braun, 1957). The titania coated samples should show additionally very strong Ti-O-Si vibration at 919 cm^{-1} (Zeitler and Braun, 1957) which could not be identified in the samples. The calcined sample shows a prominent silanol (Si-OH) vibration vanishing (wavenumber 970 cm^{-1}) and only exhibit strong siloxane (Si-O-Si) vibrations. Furthermore, the broad OH peak present in non-calcined samples disappears. In conclusion, the silica network is stabilized due to the higher degree of condensation and the resulting lesser affection by nucleophilic attack of water (Cypryk and Apeloig, 2002. Although from literature it can be expected that the surface rehydroxylates (Zhuravlev, 2000, Warring et al., 2016), i.e. the effect of calcination is reversible, we did not experience such a rehydroxylation within 4 weeks, as there was no loss of functionality of the surface improvement strategy. However, the negative side effect of calcination is the loss of fluorescence of the organic fluorophore (dye) which cannot withstand high temperatures (500 – 700 °C).

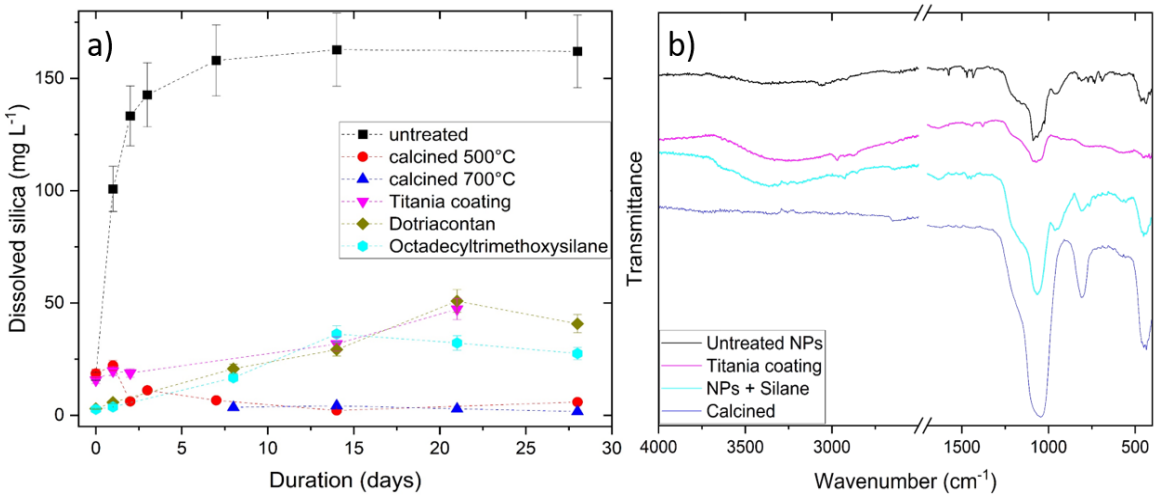

Figure 5: A) Impact on the dissolution behavior of silica nanoparticles by testing different stability improvement strategies over 4 weeks. The untreated nanoparticles show the expected behavior, an immediate dissolution and reaches the silica saturation concentration, whereas the treated particles show only minor dissolution and seem to equilibrate far below saturation. B) shows the FT-IR ATR spectra of untreated particles and surface modified particles.

3.3. Sorption

Sorption is a ubiquitous problem when conducting tracer experiments (Kasnavia et al., 1999). In hydrology, it is usually advisable to use tracers that have favorable sorption properties, e.g., uranine, eosin, sodium naphthionate, etc. (Flury and Wai, 2003). However, in geothermal reservoir exploration, two factors may be drastically different from hydrologic aquifer tests: temperature and salinity of the fluids (Chrysikopoulos, 1993). Preliminary sorption tests at 80 °C using eosin showed sorption of about 55 % on coarse quartz sand in distilled water and 4 M NaCl solution, while using a natural clayey sediment under the same conditions increased sorption to 67 % and 100 % in distilled water and 4 M NaCl solution, respectively. These results are consistent with room temperature sorption tests of eosin performed by Magal et al. (2008). Corresponding tests for sorption of nanoparticle tracers at high temperatures are in preparation.

We evaluate our nanoparticle tracer in terms of flow performance at higher salinity. Figure 6 shows the intensities of the breakthrough curves normalized to the breakthrough curve in pure water (Fig. 6a). The addition of 10 g NaCl per liter lowers the breakthrough curve to about one-third, indicating strong retention and sorption within the sand-filled column due to the presence of dissolved salts. This behavior is consistent with the data of Liu et al. (1995). The affinity of the nanoparticles to adhere to quartz grains in electrolyte solutions can be explained by surface charges (Liu et al., 2020). Initially, the nanoparticle tracers have a negative ζ-potential (~ -34 mV), as do the quartz grains. In the absence of cationic ions in the solution, sorption is unlikely, whereas in the presence of a cationic ion (in this case sodium), the ions can affect the electrostatic interactions between particles and matrix, promoting adsorption, adhesion and retention (Buoyer et al., 2001, Franks, 2002, Pianegonda et al., 2005).

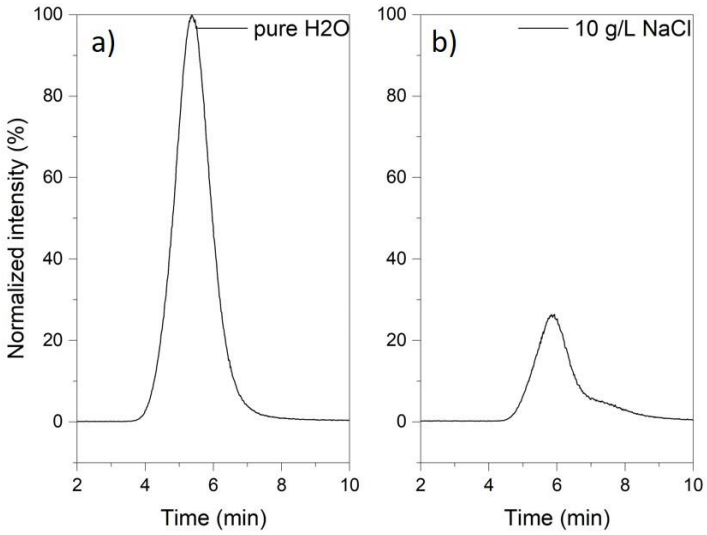

Figure 6: Breakthrough curves of nanoparticle tracers in flow through tests in coarse quartz sand using pure water (Millipore) and a 10 g L^{-1} NaCl solution. The curves are normalized on the breakthrough curve in pure water. The retention of the particles increases by about 70 % when salt is present in solution.

3.4 Sorption control

Consequently, one approach to controlling the sorption of our nanoparticles would be to modify the ζ-potential of the particles so that they are either nearly neutral or have the opposite charge to the sand grains. Surfactants, especially anionic and cationic are known to affect effectively the surface charge of silica nanoparticles (Ahualli et al., 2011). To test the performance of such modification methods, four different additives were tested by monitoring the change in the nanotracer breakthrough curves. Sodium dodecyl sulfate (SDS), an anionic surfactant, cetyltrimethylammonium bromide (CTAB), a cationic surfactant and two zwitterionic surfactants SB3-14 (sulfobetaine 3-14, N-tetradecyl-N,N-dimethyl-3-ammonio-1-propanesulfonate) and NDSB 201 (pyridinium propylsulfonate-(1)) were chosen. While the addition of the cationic surfactant CTAB did not improve tracer breakthrough and also negatively affected the protective function of the hull, the addition of 5 g L^{-1} SDS to the 10 g L^{-1} NaCl fluid increased the recovery of nanoparticle tracers to 175 % (Fig. 7a), assuming that the recovery in NaCl solution is 100 % (Fig. 6b). The addition of 20 g L^{-1} SDS further increased the recovery to 353 % (Fig. 7b). The zwitterionic surfactants increased the retrieval to 115 % (SB3-14, Fig. 7c) and 162 % (NDSB 201, Fig. 7d). Although the zwitterionic surfactants appear to have lower efficacy in controlling sorption, they are dosed about ten times lower than the anionic surfactant. However, from an economic point of view, the use of SDS is most advisable.

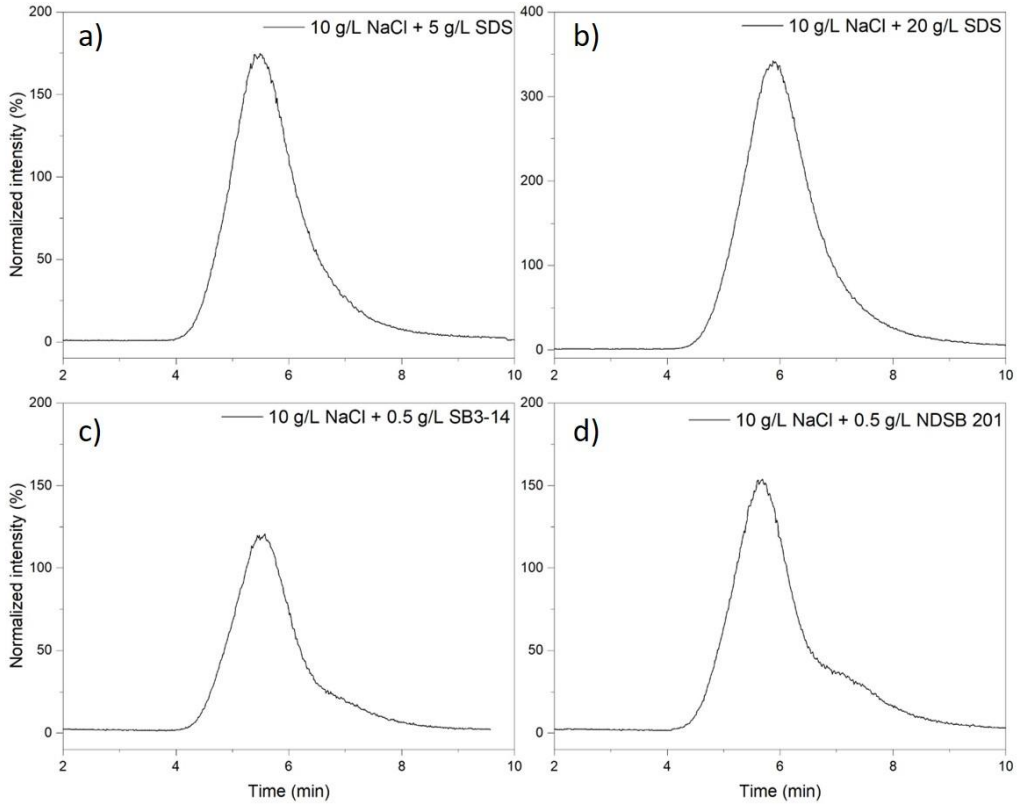

Figure 7: Breakthrough curves of nanoparticle tracers in 10 g L NaCl solution with addition of various surfactants. The intensity is normalized on the breakthrough curve of nanoparticle tracers in 10 g L NaCl solution. Please note the y-axis change in b).

CONCLUSION AND PROSPECTS

We presented the development and proof-of-concept of a novel type of nanoparticles-based tracers for simultaneous flow path and temperature detection in geothermal reservoirs. The ~70 nm-sized nanotracers are designed by a three-layered architecture, namely a fluorescent core, a fluorescently doped mesoporous shell and a protective, temperature-triggered hull. This concept has the advantage of being modular and accurately detecting temperature due to the sharp threshold of the temperature-triggered hull. We evaluated the performance comparing the breakthrough curves of nanotracers through a quartz-sand filled flowthrough column to breakthrough curves of uranine and eosin. We further identified the hydrothermal instability and the sorption on reservoir medium to be the most critical issues when applying nanotracers as tracers for geothermal reservoirs. To overcome these challenges, we provide and proof the effectiveness of a variety of stabilization methods (chemical surface modifications, strengthening the silica network, etc.) and control sorption rate through addition of surfactants. Further approaches would be adapting the structuring process of the nanotracers amplifying their application field and monitoring the ζ-potential and surface interactions of particles, reservoir fluids and different reservoir rocks.

ACKNOWLEDGEMENTS

This study is part of the subtopic "Geoenergy" in the program "MTET - Materials and Technologies for the Energy Transition" of the Helmholtz Association. The support from the program is gratefully acknowledged.

REFERENCES

Ahualli, S., Iglesias, G. R., Wachter, W., Dulle, M., Minami, D., and Glatter, O.: Adsorption of Anionic and Cationic Surfactants on Anionic Colloids: Supercharging and Destabilization. Langmuir, 27, (2011), 15, 9182 – 9192.

Alaskar, M., Ames, M., Liu, C., Li, K, and Horne, R.: Temperature nanotracers for fractured reservoir characterization. Journal of Petroleum Science and Engineering, 127, (2015), 17.

Alexander, G. B., Heston, W. M., and Iler, R. K.: The solubility of amorphous silica in water. J. Phys. Chem. 58, (1954), 3.

Buoyer, F., Robben, A., Yu, W. L., and Borkovec, M.: Aggregation of Colloidal Particles in the Presence of Oppositely Charged Polyelectrolytes: Effect of Surface Charge Heterogeneities. Langmuir, 17, (2001), 5225 – 5231.

Chrysikopoulos, C.V.: Artificial tracers for geothermal reservoir studies. Geo 22, (1993), 60 – 70.

Crundwell, F. K.: On the Mechanism of the Dissolution of Quartz and Silica in Aqueous Solutions. ACS Omega, 2, (2017), 12.

Cypryk, M., and Apeloig, Y.: Mechanism of the Acid-Catalyzed Si-O Bond Cleavage in Siloxanes and Siloxanols. A Theoretical Study. Organometallics, 21, (2002), 2165 – 2175.

Flury, M., and Wai, N.N.: Dyes as tracers for vadose zone hydrology. Reviews of Geophysics, 41 (1), (2003), 2-1 – 2-37.

Franks, G. V.: Zeta Potentials and Yield Stresses of Silica Suspensions in Concentrated Monovalent Electrolytes: Isoelectric Point Shift and Additional Attraction. Journal of Colloid and Interface Science 249, (2002), 44 - 51.

Iler, R. K.: The chemistry of silica. Solubility, Polymerization, Colloid and Surface Properties, and Biochemistry. John Wiley & Sons, (1979).

Jafari, S., Derakhshankhah, H., Alaei, L., Fattahi, A., Varnamkhasti, B. S., and Saboury, A. A.: Mesoporous silica nanoparticles for therapeutic/diagnostic applications. Biomed Pharmacother., 109, (2019), 1100 – 1111.

Kasnavia, T., Vu, D., and Sabatini, D.: Fluorescent Dye and Media Properties Affecting Sorption and Tracer Selection. Ground Water, 37, 3, (1999), 376 - 381.

Kittilä, A., Jalali, M. R., Evans, K. F., Willmann, M., Saar, M. O., Kong, X.-Z.: Field Comparison of DNA-Labeled Nanoparticle and Solute Tracer Transport in a Fractured Crystalline Rock. Water Resources Research, 55, (2019), 8, 6577 – 6595.

Kong, X.-Z., Deuber, C. A., Kittilä, A., Somogyvári, M., Mikutis, G., Bayer, P., Stark, W. J., and Saar, M. O.: Tomographic Reservoir Imaging with DNA-Labeled Silica Nanotracers: The First Field Validation. Environmental Science & Technology, 52, (2018), 23, 13681 – 13689.

Liu, D., Johnson, P. R., and Elimelech, M.: Colloid Deposition Dynamics in Flow Through Porous Media: Role of Electrolyte Concentration. Environ. Sci. Technol., 29, (1995), 2963 – 2973.

Liu, G., Zhong, H., Ahmad, Z., Yang, X., and Huo, L.: Transport of engineered nanoparticles in porous media and its enhancement for remediation of contaminated groundwater. Critical Reviews in Environmental Science and Technology, 50:22, (2020), 2301 – 2378.

Magal, E.; Weisbrod, N.; Yakirevich, A., and Yechieli, Y.: The use of fluorescent tracers in highly saline groundwater. Journal of Hydrology, 358, (2008), 124-133.

Maier, F., Schaffer, M., and Licha, T.: Temperature determination using thermo-sensitive tracers. Experimental validation in an isothermal column heat exchanger. Geothermics, 53, (2015), 533 – 539.

Mikutis, G., Deuber, C. A., Schmid, L., Kittilä, A., Lobsiger, N., Puddu, M, Asgeirsson, D. O., Grass, R. N., Saar, M. O., and Stark, W. J.: Silica-Encapuslated DNA-Based Tracers for Aquifer Characterization. Environ. Sci. Technol. 52, (2018), 12142 – 12152.

Möller, K., and Bein, T.: Degradable Drug Carriers: Vanishing Mesoporous Silica Nanoparticles. Chem. Mater., 31, (2019), 12, 4364 – 4378.

Pianegonda, S., Barbosa, M. C., and Levin, Y.: Charge reversal of colloidal particles. Europhysics Letters ,(2005).

Puddu, M., Mikutis, G., Stark, W. J., and Grass, R. N.: Submicrometer-Sized Thermometer Particles Exploiting Selective Nucelic Acid Stability. Small, 12, (2016), 4, 452 – 456.

Rudolph, B., Berson, J., Held, S., Nitschke, F., Wenzel, F., Kohl, T., and Schimmel, T.: Development of thermo-reporting nanoparticles for accurate sensing of geothermal reservoir conditions. Scientific reports, 10, (2020), 1, 1 – 7.

Socrates, G.: Infrared and Raman Characteristic Group Frequencies: Tables and Charts. John Wiley & Sons, (2004).

Spitzmüller, L., Nitschke, F., Rudolph, B., Berson, J., Schimmel, T., and Kohl, T.: Dissolution Control and Stability Improvement of Silica Nanoparticles in Aqueous Media. Journal of Nanoparticle Research, (2023), 10.1007/s11051-023-05688-4.

Stephens, D. B., Hsu, K.-C., Prieksat, M. A., Ankeny, M. D., Blandford, N., Roth, T. L., Kelsey, J. A., and Whitworth, J. R.: A comparison of estimated and calculated effective porosity. Hydrogeology Journal, 6, (1998), 156 – 165.

Vitorge, E., Szenknect, S., Martins, J. M. F., Barthès, V., and Gaudet, J.-P.: Comparison of three labeled silica nanoparticles used as tracers in transport experiments in porous media. Part II: Transport experiments and modeling. Environmental Pollution, 184, (2014), 613 – 619.

Warring, S. L., Beattie, D. A., and McQuillan, A. J.: Surficial Siloxane-to-Silanol Interconversion during Room-Temperature Hydration/Dehydration of Amorphous Silica Films Observed by ATR-IR and TIR-Raman Spectroscopy. Langmuir, 32, (2016), 6, 1568 – 1576.

Widjornako, D. M., Kartini, J. I., and Nuryono: Phosphonate modified silica for adsorption of Co(II), Ni(II), Cu(II), and Zn(II). Indo. J. Chem., 14, (2014), 2, 143 – 151.

Zeitler, V. A., and Brown, C. A.: The infrared spectra of some Ti-O-Si, Ti-O-Ti and Si-O-Si compounds. J. Phys. Chem., 61, (1957), 9, 1174 – 1177.

Zhang, Y., Manley, T. S., Li, K., and Horne, R. N.: Uniquely identifiable DNA-embedded silica nanotracer for fractured reservoir characterization. Proceedings of the 41st Workshop on Geothermal Reservoir Engineering, Stanford University, CA, (2016).

Zhuravlev, L. T.: The chemistry of amorphous silica. Zhuravlev model. Colloids and Surfaces A: Physicochemical and Engineering Aspects 173, (2000), 1-38.